WALL RESOLUTION STUDY FOR DIRECT NUMERICAL SIMULATION OF TURBULENT CHANNEL FLOW USING A MULTIDOMAIN CHEBYSHEV GRID

Zia Ghiasi sghias2@uic.edu
Dongru Li dli21@uic.edu
Jonathan Komperda jonk@uic.edu
Farzad Mashayek mashayek@uic.edu

Department of Mechanical and Industrial Engineering
University of Illinois at Chicago
842 W. Taylor Street. Chicago, Illinois 60607, United States

ABSTRACT

In wall-bounded turbulent flows, the near-wall region is the most sensitive to the grid resolution. An insufficient resolution normal to the wall results in an inadequate prediction of flow statistics. Channel flow is a well-studied benchmark for wall-bounded turbulent flows. The grids used in previous direct numerical simulations (DNS) of turbulent channel flow satisfy two general conditions: (1) The first point (nearest to the wall) is located within $y^+ < 1$ (y^+ is the non-dimensional wall coordinate), and (2) there are at least 10 points within $y^+ < 10$. In numerical schemes that use a nonuniform distribution of grid points normal to the wall, satisfying both conditions demands more consideration. The discontinuous spectral element method (DSEM), as an example, uses a multidomain staggered grid with Chebyshev distribution of points inside non-overlapping subdomains. In each subdomain, the first and last grid's size is much smaller than the average grid size within that subdomain. Satisfying the second condition in such a method results in an excessively small mesh size at the wall, restricts the time step size, and increases the computational cost of the simulation. In this paper, DSEM is used to conduct DNS of compressible, turbulent flow in a three-dimensional channel to investigate the sufficient near-wall resolution, while minimizing the restriction of the time step size. The first- and second-order statistics are used to assess the accuracy of the simulations.

INTRODUCTION

The accuracy of predicting near-wall turbulence statistics in direct numerical simulations (DNS) strongly depends on the adequacy of the spatial resolution normal to the wall. The grid spacing criteria should be independent of Reynolds number. Therefore, the spatial spacing is calculated based on the wall unit (y^+). Previous DNS studies of turbulent channel flow employ grids that satisfy two general criteria: (1) The first point (nearest to the wall) is located at $y^+ < 1$, and (2) there are at least 10 points below $y^+ = 10$. In a finite difference scheme (or any other scheme that is capable of employing a uniform or nearly uniform grid), these requirements can be satisfied by placing the first point within the first wall unit and increasing the spacing gradually moving away from the wall. However, in the schemes that use nonuniform grids, such as some types of spectral and spectral element methods, because of the special distribution of the grid points, by satisfying the second criterion, the size of the first grid is usually orders of magnitude smaller than $y^+ = 1$. For example, in discontinuous spectral element method (DSEM) (Kopriva & Kolias, 1996; Kopriva, 1998, 2009) the domain is divided into non-overlapping hexahedral subdomains (the so-called elements). Inside each element, the spectral approximation is applied using Lagrange polynomials with an order of approximation P. A staggered grid with a Chebyshev distribution of points is used inside each element. The grid consists of Gauss quadrature points (used to calculate the solutions) and Gauss-Lobatto quadrature points (used to calculate fluxes). Each hexahedral element in the physical space is mapped into a unit cube in the computational space.

The solution (Gauss) points of an element with a Chebyshev distribution of points are determined by

$$\overline{X}_{j+1/2} = \frac{1}{2}\left[1 - \cos\left(\frac{2j+1}{2P+2}\pi\right)\right], \quad j = 0, \ldots, P, \quad (1)$$

in each direction, over the interval of $[0,1]$ in the mapped space. For example, for $P = 9$, such a unit element has 10 points in each direction, with a distribution of the points as illustrated in Fig. 1. Note that the first grid point is located at $\overline{X}_{1/2} = 6.16 \times 10^{-3}$. If we set the size of the nearest element to the wall such that its first point is located at $y^+ = 1$, there would be only 2 points within $y^+ < 10$. Even by placing the first point at $y^+ = 0.1$, there would be only 6 points below $y^+ = 10$. On the other hand, if the first element is placed such that the second criterion is satisfied, i.e., there are 10 points below $y^+ = 10$, then the first point would be located at $y^+ = 0.0616$. In this case, the minuscule grid spacing (which happens both on the wall side and the other end of the first element) requires an excessively small time step size and significantly adds to the computational cost. Therefore, for schemes that use Chebyshev grids, it is challenging to balance between the two requirements and choose a near-wall resolution that is sufficient to capture the flow characteristics, while minimizing the computational cost. To the best knowledge of the authors, this

challenge has not been tackled before. In this paper, a compressible, turbulent flow in a periodic channel is simulated to investigate the appropriate near-wall resolution and the effect of the resolution on the computational cost of the simulation.

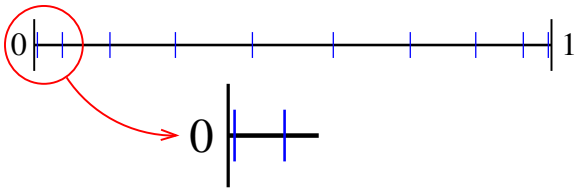

Figure 1. Distribution of Gauss points (blue ticks) in a Chebyshev grid of order $P = 9$.

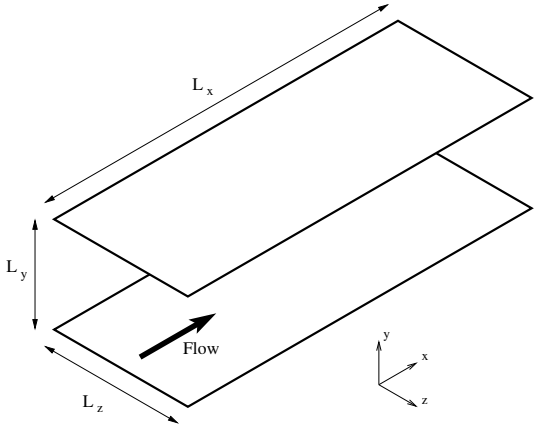

Figure 2. Schematic of the computational domain.

NUMERICAL METHODOLOGY

In this work, a nodal collocation form of the DSEM is used as the flow solver (Jacobs, 2003). The DSEM code has been employed for DNS and large eddy simulations (LES) of compressible flow in complex geometries (Li *et al.*, 2016; Ghiasi *et al.*, 2016). The code solves the unsteady, compressible Navier-Stokes equations in non-dimensional conservative form. The governing equations can be written in a vector form as

$$\vec{Q}_t + \vec{F}^a_x + \vec{G}^a_y + \vec{H}^a_z = \frac{1}{Re_f}(\vec{F}^v_x + \vec{G}^v_y + \vec{H}^v_z). \qquad (2)$$

Here, $\vec{Q}$ is the solution vector, which is given by $\vec{Q}^T = [\rho \quad \rho u \quad \rho v \quad \rho w \quad \rho e]$, where ρ is the density; u, v, and w are the three components of velocity; e is the sum of the internal and kinetic energy per unit mass. In Eq. 2, $\vec{F}^a$, $\vec{G}^a$, and $\vec{H}^a$ are the advective fluxes, and $\vec{F}^v$, $\vec{G}^v$, and $\vec{H}^v$ are the viscous fluxes as described in Jacobs (2003). Three non-dimensional numbers, i.e., reference Reynolds number (Re_f), reference Mach number (Ma_f), and reference Prandtl number (Pr_f) appear in the dimensionless governing equations, and are defined by

$$Re_f = \rho^*_f L^*_f u^*_f / \mu^*, \qquad (3)$$

$$Ma_f = u^*_f / c^*_f, \qquad (4)$$

$$Pr_f = c^*_p \mu^* / k^*, \qquad (5)$$

based on the reference length L^*_f, density ρ^*_f, velocity u^*_f, and temperature T^*_f scales. The superscript $*$ denotes dimensional variables. In the above equations, μ^* and k^* are the fluid's dynamic viscosity and conductivity coefficients, respectively; c^*_p is the constant pressure specific heat of the fluid, and $c^*_f = \sqrt{\gamma R^* T^*_f}$ is the reference speed of sound, where $\gamma = 1.4$ is the heat capacity ratio, and R^* is the gas constant. The pressure, p^*, is calculated using the equation of state, $p^* = \rho^* R^* T^*$ that closes the Navier-Stokes equations. A low-storage, fourth-order, explicit Runge-Kutta scheme is used for time integration.

PERIODIC CHANNEL FLOW SIMULATION

In this work, the DSEM code is used to conduct DNS of a three-dimensional, compressible, subsonic, fully developed turbulent flow in a periodic channel to study the grid resolution requirement near the wall. First- and second-order statistics of the flow near the wall are used to assess the accuracy of the solution.

A schematic of the computational domain and the coordinate system is shown in Fig. 2. The flow is periodic in streamwise (x) and spanwise (z) directions, and no-slip walls are used at the normal (y) boundaries. The dimensions of the computational domain are $L_x = 5.61$, $L_y = 2$, and $L_z = 2$ in the streamwise, normal, and spanwise directions, respectively. The lengths are scaled by the channel half-height ($\delta = L_y/2$). This choice of domain allows for comparison with previous work.

Previous Grids of Channel Flow DNS

Turbulent flow in a periodic channel with the configuration described in the previous section has been numerically studied before. Kim *et al.* (1987) performed the DNS of a turbulent channel flow at a friction Reynolds number of $Re_\tau = u_\tau \delta/\nu = 180$ (u_τ is the wall friction velocity). They used a fully spectral method with Fourier series in the homogeneous directions and a Chebychev polynomial expansion in the normal direction. Their grid had 12 points within $y^+ < 10$, and the first point was located at $y^+ = 0.05$. Rai & Moin (1991) presented a finite-difference solution to the turbulent channel flow ($Re_\tau = 180$) to compare the results with those obtained from spectral methods. In their grid, the distribution of the points normal to the wall followed a geometric progression. Lyons *et al.* (1991) presented a pseudospectral technique and simulated the turbulent channel flow with heat transfer for a friction Reynolds numbers of $Re_\tau \approx 130$. Their grid's first point was located at $y^+ = 0.18$. Crawford (1996) conducted a resolution study for turbulent simulations using spectral elements by simulating a fully turbulent channel flow at $Re_\tau \approx 200$. They also used a Fourier discretization in the the periodic directions and a Chebyshev expansion in the normal direction with the first grid point located at $y^+ = 0.29$. Moser *et al.* (1999) presented detailed statistical data for DNS of turbulent channel flow at three different Reynolds numbers of $Re_\tau = 180$, 395, and 590. In all three cases, there were 13 or more grid points below $y^+ = 10$. Lee & Moser (2015) recently presented a DNS of incompressible, turbulent channel flow at different Reynolds numbers ranging from $Re_\tau = 180$ to 5,186. They had 15 points below $y^+ = 10$ for the highest Reynolds number case. The first point was located at $y^+ = 0.074$ and $y^+ = 0.498$ for their lowest and highest Reynolds number cases, respectively. A summary of the previously mentioned

work with more details of their computational domains are included in Table 1. All domain lengths are scaled by the channel half-height (δ), and domain sizes and grid points appear in the order x, y, z.

Flow Conditions

In the present resolution study, we consider the channel flow with a friction Reynolds number of $Re_\tau \approx 210$. This friction Reynolds number corresponds to a Reynolds number of $Re = 5,000$ based on the channel half-height (δ) and the centerline velocity (U_l) of a laminar parabolic profile with the same volumetric flux. The Reynolds number based on the channel half-height and the bulk mean velocity in the channel ($\overline{U}$) is $Re_f = 3,333$. The volumetric flux (Q) can be calculated by

$$Q = \int_{A_{cs}} u \, \mathrm{d}A = \frac{2}{3} A_{cs} \, U_l = A_{cs} \, \overline{U}, \tag{6}$$

where $A_{cs} = L_y L_z$ is the cross-sectional area. The Mach number, based on the bulk velocity, is $Ma = 0.4$, and the reference Prandtl number is chosen to be $Pr_f = 0.72$.

In a channel flow, the flow is sustained by a negative pressure gradient, which is not possible with a periodic domain in the streamwise direction. Therefore, a forcing term is required to maintain the flow. Lenormand *et al.* (2000) showed that a time-dependent forcing term is needed to achieve a time-independent mass flux for a compressible flow. The forcing algorithm of Lenormand *et al.* (2000) is used in this work.

Initialization and Transition to Turbulence

The velocity field is initialized with a laminar parabolic profile with a uniformly distributed random disturbance applied to the streamwise velocity, as

$$u(y) = -6 \left[\left(\frac{y}{2} \right)^2 - \left(\frac{y}{2} \right) \right] (1 + \varepsilon). \tag{7}$$

Here, ε is a 10% random disturbance which is introduced to accelerate the transition of the flow regime to turbulence. The temperature is initialized with a laminar Poiseuille profile, and the density has an initial constant value of $\rho_0 = 1$. The initial pressure is calculated through the ideal gas law.

Our preliminary tests showed that the initial disturbance gradually decays after a few flow-through times with $Re = 5,000$ for the case with the base resolution of $P = 7$, and a fully developed turbulence cannot be obtained. A temporary increase in the Reynolds number to $Re = 10,000$ does not help to preserve the initial disturbance either. Increasing the Reynolds number further is not computationally practical with a reasonable simulation time. Instead, the simulation is started at a lower resolution of $P = 2$. In this approach (Jacobs, 2003), the truncation error of the scheme at the lower resolution is expected to be sufficiently large to provide the required disturbance for a transition to turbulence. While the flow undergoes the transition to turbulence, the resolution is increased step by step ($P = 2$, $P = 3$, $P = 5$, $P = 7$), and the flow is simulated for about $3 \sim 4$ flow-through times at each resolution until the desired resolution of $P = 7$ is reached. Then, the simulation is continued at $P = 7$. First- and second-order statistics are calculated after the flow reaches the statistically stationary condition. Here, we use the skin friction coefficient (c_f)

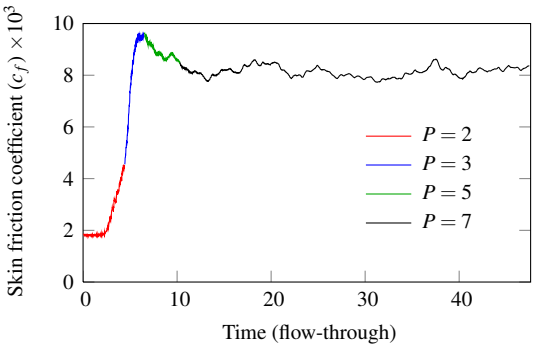

Figure 3. Changes of skin friction coefficient (c_f) in time (scaled with flow-through time) for the channel flow simulation (case A-P7).

as an indicator of reaching the statistically stationary condition. Figure 3 shows c_f of the channel flow plotted versus flow-through time ($L_x/\overline{U}$). During the first two flow-through times, the skin friction coefficient stays at the laminar value of $c_f = 6/Re_f = 1.8 \times 10^{-3}$. After that, c_f increases, which denotes transition to turbulence. After about 15 flow-through times, the skin friction coefficient levels off at a value of $c_f \approx 8.13 \times 10^{-3}$ (averaged in time), indicating statistically stationary flow. Dean (1978) provides an empirical relation for the skin friction coefficient in two-dimensional rectangular duct flows as $c_f = 0.073 Re_h^{-1/4}$, where $Re_h = \overline{U} h / \nu$ is the Reynolds number based on the bulk mean velocity ($\overline{U}$) and the channel height ($h = 2\delta$). The empirical skin friction coefficient for the current simulation would be $c_f = 8.08 \times 10^{-3}$, which is in excellent agreement with the calculated value of 8.13×10^{-3}. Results of the turbulent channel flow presented in this work are obtained using this approach.

Grid Resolution

Three simulations are conducted using three different grids for this resolution study. Details of each grid are included in Table 2. The grid used for the first simulation (case A-P7) contains 4,032 elements. The approximation order inside each element is $P = 7$. Also, 18 and 14 elements are uniformly distributed in the streamwise and spanwise directions, respectively. Sixteen elements are placed in the normal direction. The distribution of elements in the normal direction (y) follows a hyperbolic tangent function of the form

$$\frac{y_n}{L_y} = \frac{1}{2} \left(1 - \frac{\tanh\left[\lambda \left(\frac{1}{2} - \frac{n}{N_y} \right) \right]}{\tanh\left[\lambda / 2 \right]} \right), \quad 0 < n < N_y, \tag{8}$$

where y_n is the location of the boundaries of the elements, N_y is the number of elements in the normal direction, and λ is a tunable coefficient, which determines the compactness of the grid near the wall. For case A-P7, by choosing $\lambda = 3.44$, the first grid point is placed at $y^+ \approx 0.069$, and there are 11 points below $y^+ = 10$. This grid satisfies both near-wall resolution conditions and hence will serve as our base case.

As mentioned earlier, a Chebyshev grid with its first 10 points within $y^+ < 10$ requires an excessively small time step size, which makes the simulation computationally expensive. To determine whether such resolution is needed,

Table 1. Previous DNS studies of the planar turbulent channel flow.

Reference	Re_τ	Domain size	Grid points
Kim *et al.* (1987)	180	$4\pi \times 2 \times 2\pi$	$192 \times 129 \times 160$
Rai & Moin (1991)	180	$4\pi \times 2 \times 2\pi$	$64 \times 65 \times 64$
Lyons *et al.* (1991)	$125 \sim 135$	$12.67 \times 2 \times 6.33$	$128 \times 65 \times 128$
Crawford (1996)	200	$5.61 \times 2 \times 2$	$64 \times 120 \times 100$
Moser *et al.* (1999)	180, 395, 590	$4\pi \times 2 \times 4\pi/3$	$128 \times 129 \times 128$
Lee & Moser (2015)	182, 544, 1,000, 5,186	$8\pi \times 2 \times 3\pi$	$10{,}240 \times 1{,}536 \times 7{,}680$

Table 2. Details of the grids used for the three resolution study cases.

Case	Number of elements in x, y, z	P	Total grid points	First point's y^+	Points within $y^+ < 10$	Time step size	Re_τ
A-P7	$18 \times 16 \times 14$	7	2,064,384	0.069	11	6.48×10^{-4}	213.6
B-P7	$18 \times 14 \times 14$	7	1,806,336	0.133	5	1.00×10^{-3}	203.8
A-P9	$18 \times 16 \times 14$	9	4,032,000	0.045	13	4.16×10^{-4}	215.2

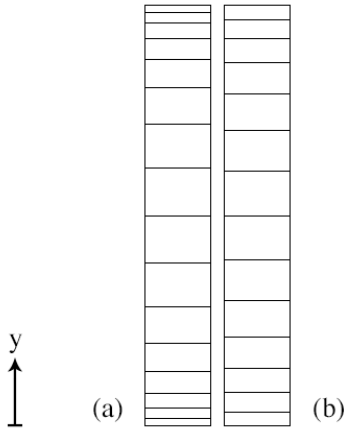

Figure 4. Distribution of elements in the wall normal direction for (a) case A-P7 and (b) B-P7.

and how severely it affects the computational cost, the second case (B-P7) with lower normal resolution near the wall is designed. In the case B-P7, the sizes of the first two elements near the wall in the normal direction are almost twice those in case A-P7. In this grid, the first grid point is placed at $y^+ \approx 0.133$ (compare with $y^+ \approx 0.069$ for case A-P7), and there are five (compare with 11 for case A-P7) points within $y^+ < 10$. Here, we are interested in the grid resolution near the wall only. Therefore, the resolution away from the wall is maintained. To achieve this, the tunable coefficient in Eq. (8) is chosen to be $\lambda = 2.525$, and the number of elements in the normal direction is reduced to 14. Figure 4 compares the distribution of elements in the normal direction for case A-P7 and B-P7.

In order to validate the adequacy of the resolution of case A-P7, a third case (case A-P9) is designed such that it has higher spatial resolution than case A-P7 in all three directions. Spectral element methods provide two levels of control over spatial resolution refinement, i.e., h-refinement and p-refinement. With h-refinement, the number of elements, and subsequently sizes of the elements, are changed. However, with p-refinement, the elements remain unchanged, and the order of approximation (P) within the elements is modified. Case A-P9 uses the same elements as the case A-P7. However, the polynomial order is increased to $P = 9$. Case A-P9 has almost twice the total number of grid points of case A-P7. The results for the three cases are provided and discussed in the next section.

Results and Discussions

Examples of the two-point velocity correlation for the base case (case A-P7) are shown in Fig. 5 to illustrate the adequacy of the computational domain. In this figure, two-point correlations in the streamwise and spanwise directions at two different distances from the wall (one very close to the wall and one away from the wall, near the core of the channel) fall off within the range of $|R_{ii}| < 0.05$ for the largest separation, where R_{ii} is the two-point correlation of the component of velocity in the i-direction. This observation confirms that the values of the three velocity components are independent at the largest separation, and the computational domain is sufficiently large in both periodic directions to capture the largest scale of the flow. This behavior was observed in all simulations.

The mean streamwise velocity profiles for all three cases in this resolution study as well as the previous DNS of Crawford (1996) are shown in Fig. 6. Velocities are scaled with the friction velocity (u_τ), and the wall coordinate (y^+) is plotted on a logarithmic scale. The plot demonstrates that all three cases have the same mean streamwise profiles, and those profiles agree with the previous simulation. All profiles also follow the law of the wall. It is therefore concluded that all three cases have sufficient resolution to predict the first-order statistics of the near-wall flow accurately.

Comprehensive grid convergence can only be claimed with the verification of second-order statistics. It is shown that under-resolved grid in one or more directions negatively affects the prediction of the mean properties as well higher-order statistics of the flow (Karniadakis & Sherwin, 1999). Figure 7 presents the root-mean-square (RMS) of the three components of velocity for all cases, along with the results from DNS of Crawford (1996). The values from case A-P7 and case A-P9 are within 4% of each other, and they both provide close agreement with the reference re-

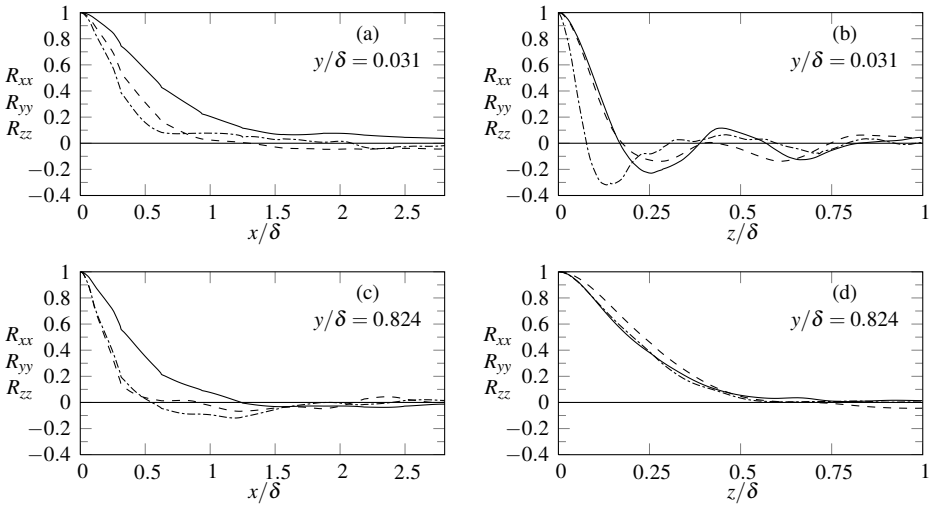

Figure 5. Two-point correlations of the velocity from the periodic channel flow: R_{xx} (——), R_{yy} (- - -), R_{zz} (-·-·-·) in the streamwise (near the wall (a) and away from the wall (c)) and spanwise (near the wall (b) and away from the wall (d)) directions.

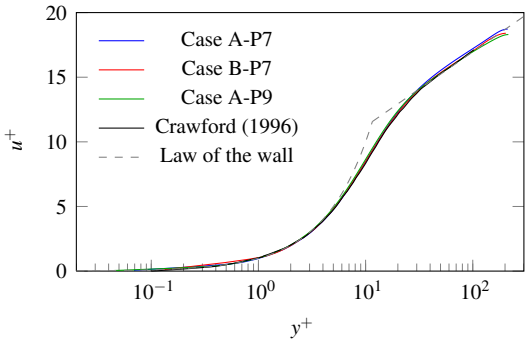

Figure 6. Comparison of mean streamwise velocity profiles obtained on different grids with published data.

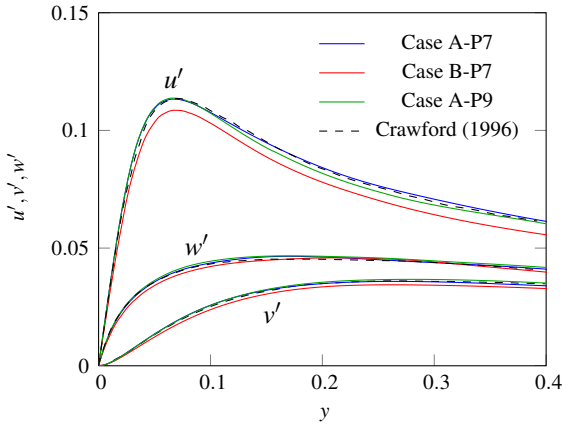

Figure 7. Comparison of RMS velocity profiles obtained on different grids with published data.

sults, which means that case A-P7 provides sufficient resolution to predict velocity RMS profiles. Even though case B-P7 predicts the mean velocity correctly, it underpredicts the RMS velocity near the wall. This underprediction is more evident in the streamwise direction (u'). This observation is consistent with the results of Crawford (1996). Their simulations revealed that the low resolution in the normal direction causes underprediction of streamwise turbulence intensity.

Moreover, from Table 2 it can be seen that Re_τ, which is calculated using the wall friction velocity obtained from the simulations, does not change significantly from A-P7 to A-P9. However, the Re_τ of case B-P7 is noticeably lower than those of the other two cases. Therefore, based on comparisons of mean velocity, RMS velocity, and Re_τ, we conclude that the resolution in case A-P7 is sufficient to predict the correct first- and second-order statistics, and case B-P7 does not provide sufficient resolution.

In wall-bounded turbulent flows, the grid near the wall should be sufficiently resolved to capture the behavior of the velocity profile in all regions of the boundary layer: the viscous (laminar) sublayer, the buffer layer, and the fully turbulent region (log-law region). Figure 8 shows the location of grid points normal to the wall for all three cases superimposed on the plot of the friction velocity based on the law of the wall to visualize the position of the points with respect to the boundary layer. In this figure, points from only the first three elements near the wall are shown. For case B-P7, there are 5 grid points within $y^+ < 10$ and only 3 points inside the laminar sublayer ($y^+ < 5$). However, case A-P7 and A-P9 have 11, and 13 grid points within $y^+ < 10$, respectively, and they both have 7 points within the laminar sublayer.

The small grid size at the wall results in a highly restricted time step size. The time step size required by the three cases are presented in Table 2. The time step size for case A-P7 is 35% smaller than that of case B-P7. The computation times for cases B-P7, A-P7, and A-P9 are 89, 160, and 289 minutes per flow-through time, respectively. The simulations were run on 32 nodes with Intel Xeon E5-2670 (2.60 GHz) with 16 cores in each node. The computation cost increases for each case based on the resolution of the grid due to two reasons: (1) By increasing the spatial resolution, the minimum grid size, and accordingly the time step size, decrease. Therefore, more iterations are needed to complete one flow-through time of the simulation. (2) With higher resolution, there are more solution points throughout the domain that need to be updated at each time step. Therefore, the computation time required for each time step

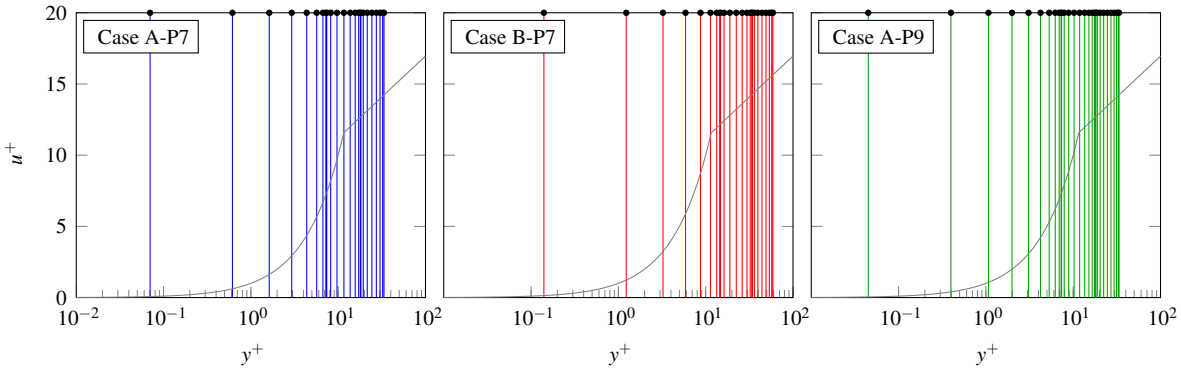

Figure 8. Location of grid points (within the first three elements near the wall) normal to the wall (vertical lines) superimposed on the plot of the friction velocity based on the law of the wall (gray curve).

increases with the resolution.

SUMMARY AND CONCLUSIONS

The grids used for previous DNS studies of turbulent channel flow satisfy two general requirements near the wall, i.e., the nearest point to the wall is within $y^+ < 1$, and there are at least 10 points below $y^+ = 10$. Satisfying the second condition in numerical methods that use nonuniformly distributed grid points, such as spectral and spectral element methods that use a Chebyshev distribution of collocation points, results in over-satisfying the first condition, i.e., excessively small minimum grid size, and significantly increases the computational cost. On the other hand, satisfying only the first criterion results in an insufficient number of points within $y^+ < 10$, and damages the prediction of the flow statistics.

DNS of a three-dimensional, compressible, fully developed turbulent flow in a periodic channel has been conducted to study the grid resolution requirement near the wall in discontinuous spectral element method with multidomain Chebyshev grid. It is shown that both conditions remain valid for such scheme. Even if the first grid point is located very close to the wall ($y^+ \ll 1$), the lack of the sufficient number of grid points within $y^+ < 10$ results in underprediction of the streamwise turbulence intensity and the friction Reynolds number, for an order of approximation of $P = 7$. Therefore, the second recommendation is required to be satisfied for accurate prediction of flow statistics, even though it results in a small minimum grid size and increases the computational cost. Further investigation is needed to study the effect of the approximation order on the near-wall resolution requirement.

ACKNOWLEDGMENTS

The computational resources for this study were provided by the UIC Extreme (High Performance Computing Cluster) at the University of Illinois at Chicago.

REFERENCES

Crawford, C. H. 1996 Direct numerical simulation of near-wall turbulence - passive and active control. Ph.D. Thesis, Princeton University.

Dean, R. B. 1978 Reynolds number dependence of skin friction and other bulk flow variables in two-dimensional rectangular duct flow. *Journal of Fluids Engineering* **100** (2), 215–223.

Ghiasi, Z., Komperda, J., Li, D. & Mashayek, F. 2016 Simulation of supersonic turbulent non-reactive flow in ramp-cavity combustor using a discontinuous spectral element method. AIAA Paper, 2016-0617.

Jacobs, G. B. 2003 Numerical simulation of two-phase turbulent compressible flows with a multidomain spectral method. Ph.D. Thesis, University of Illinois at Chicago.

Karniadakis, G. E. & Sherwin, S. J. 1999 *Spectral/hp Element Methods for CFD*. New York, NY: Oxford University Press.

Kim, J., Moin, P. & Moser, R. D. 1987 Turbulent statistics in fully developed turbulent channel flow at low Reynolds number. *Journal of Fluid Mechanics* **177**, 133–166.

Kopriva, D. A. 1998 A staggered-grid multidomain spectral method for the compressible Navier-Stokes equations. *Journal of Computational Physics* **244**, 142–158.

Kopriva, D. A. 2009 *Implementing spectral methods for partial differential equations: Algorithms for scientists and engineers*. Springer Science & Business Media.

Kopriva, D. A. & Kolias, J. H. 1996 A conservative staggerd-grid Chebyshev multidomain method for compressible flows. *Journal of Computational Physics* **125**, 244–261.

Lee, M. & Moser, R. D. 2015 Direct numerical simulation of turbulent channel flow up to $Re_\tau \approx 5200$. *Journal of Fluid Mechanics* **774**, 395–415.

Lenormand, E., Sagaut, P. & Ta Phuoc, L. 2000 Large eddy simulation of subsonic and supersonic channel flow at moderate reynolds number. *International Journal for Numerical Methods in Fluids* **32** (4), 369–406.

Li, D., Ghiasi, Z., Komperda, J. & Mashayek, F. 2016 The effect of inflow mach number on the reattachment in subsonic flow over a backward-facing step. AIAA Paper, 2016-2077.

Lyons, S. L., Hanratty, T. J. & McLaughlin, J. B. 1991 Large-scale computer simulation of fully developed turbulent channel flow with heat transfer. *International Journal for Numerical Methods in Fluids* **13** (8), 999–1028.

Moser, R. D., Kim, J. & Mansour, N. N. 1999 Direct numerical simulation of turbulent channel flow up to $Re_\tau = 590$. *Physics of Fluids* **11** (4), 943–945.

Rai, M. M. & Moin, P. 1991 Direct simulations of turbulent flow using finite-difference schemes. *Journal of Computational Physics* **96** (1), 15–53.